Mon. Not. R. Astron. Soc. **391,** 675–684 (2008) doi:10.1111/j.1365-2966.2008.13833.x

Sphere of influence and gravitational capture radius: a dynamical approach

R. A. N. Araujo,[1⋆] O. C. Winter,[1,2⋆] A. F. B. A. Prado[1⋆] and R. Vieira Martins[3⋆]

[1] *Instituto Nacional de Pesquisa Espaciais, C. P. 515, CEP 12201-970 - São José dos Campos, SP, Brazil*
[2] *São Paulo State University-UNESP, Grupo de Dinâmica Orbital e Planetologia, C.P. 205, CEP 12516-410, Guaratinguetá, SP, Brazil*
[3] *Observatório Nacional, CEP 20921-400, São Cristóvão, Rio de Janeiro, RJ, Brazil*

Accepted 2008 August 13. Received 2008 July 28; in original form 2008 April 3

ABSTRACT

For problems in celestial mechanics that involve close encounters, it is necessary to determine the region where the gravitational influence of a body prevails over the influence of other bodies. From this need comes the concept of the sphere of influence. The models most used for the calculation of the radii of these spheres are the Hill sphere and the Laplace sphere. These are determined in terms of constant parameters, resulting in a fixed-size sphere, independent of the conditions of the encounter. In this paper, we present a numerical model for the sphere of influence, whose radius has been defined in terms of the initial relative velocity of the encounter, and of the mass ratio of the system considered. The same idea was applied to the delimitation of the regions where the phenomenon of temporary gravitational capture occurs, for some given initial conditions. With this goal, a numerical study was made through integrations of the restricted three-body problem and by monitoring the energy variation of the two-body problem. This study resulted in a complete mapping of the influence and capture regions, considering systems with a mass ratio from 10^{-1} to 10^{-12}, with the empirical functions for the calculation of these limits, called the capture radius and the influence radius.

Key words: methods: numerical – celestial mechanics – Solar system: general.

1 INTRODUCTION

The problem of close encounters occurs when the movement of a body takes place in the vicinity of another body, which is massive enough to be able to influence and change its orbital evolution. In the Solar system, for instance, it is known that the Sun has a much larger mass than the other bodies in it, being in gravitational terms the dominant body. The movement of a particle with relatively small mass, such as an asteroid or a spaceship, in this system, is described by the equation of its Keplerian movement around the Sun, considering the other bodies as disturbing elements. However, if at some moment this particle approaches a planet or another body with significant mass, the gravitational influence of that body will prevail temporarily over the gravitational influence from the Sun.

The concept of the sphere of influence comes from this need to restrict the region in which the gravitational influence of a body prevails over the gravitational influence of other bodies. The most known and used models of the sphere of influence are the Hill sphere (Hill 1878) and the Laplace sphere (Roy 1988). Some examples of their applications are the following: the issues of the determination of orbital stability zones, usually given in terms of the Hill radius (Hamilton & Burns 1991; Domingos, Winter & Yokoyama 2006); studies of the formation of giant planets (Kornet, Wolf & Rózyczka 2006); in particular, problems that involve orbital manoeuvres with spacecraft, as in the case of gravity-assisted or swing-by manoeuvres (Broucke 1988; Prado 2001). This type of manoeuvre has been used in space missions to explore the Solar system. Examples of some missions using the gravity-assisted manoeuvre are the following: the mission *Mariner 10*, in 1974, in which the spacecraft reached the planet Mercury, by making use of the gravity of Venus (Dunne 1974); the missions *Voyager I* and *Voyager II*, in 1977, to explore the Jovian and Saturnian systems, which made successive gravity-assisted manoeuvres with the inner planets as well as with the visited planets (Kohlhase & Penzo 1977); the *Ulysses* mission, which consisted of the exploration of the Sun and employed a gravity-assisted manoeuvre with Jupiter to achieve a trajectory extending to high solar latitudes (Wenzel et al. 1992). Recently, the *Cassini–Huygens* mission achieved its goal, reaching Saturn after some swing-by manoeuvres with Venus (twice), Earth and Jupiter (Peralta & Flanagan 1995). The success of these missions justifies the increasing interest in this manoeuvre, and consequently in the phenomena and concepts involved in close-approach problems, such as the sphere of influence and temporary gravitational capture.

⋆E-mail: ran.araujo@gmail.com; ocwinter@feg.unesp.br; prado@dem.inpe.br; rvm@on.br

It is known that the considerations and approaches made in the deduction of the Hill and Laplace sphere of influence models allow us to calculate the radii of such spheres by taking into account the mass ratio and the distance between the main bodies. As these parameters are practically constant, the radii obtained have fixed sizes. They are completely independent of the orbital evolution of a particle that is under the gravitational attraction of these two bodies. However, it is intuitive to think that by considering the relative velocity and the distance of an encounter between the particle and the secondary body, it is possible in practice to distinguish three regimes for the influence from the secondary body. The first regime consists of the temporary gravitational capture of the particle. In such a condition, the gravitational influence of the secondary body prevails over the influence of the central body and, in terms of the two-body problem energy, this phenomenon will be characterized by the signal of this energy relative to the secondary body. It is negative in the case of a captured particle, and changes to positive when it has an opened orbit around this body, which means that it has escaped from capture. The second regime takes place in the region where the particle is no longer captured, but it passes at a distance small enough to suffer a significant influence, which is characterized by a variation in the two-body problem particle-central body energy. As this distance becomes larger, the gravitational influence decreases, until it has a value that can be considered not so significant, and an approximation of the two-body problem particle-central body can be made (third regime).

Thus, based on such characteristics, we can think in terms of a new model of the sphere of influence, obtained through the analysis of the variation of energy of the two-body problem, and given as a function of the relative velocity of the encounter.

(i) When the relative velocity is high, such a sphere of influence radius is smaller.

(ii) When such a velocity is small, the sphere of influence radius is larger.

Taking this into account, in this paper we present a new approach. Here, we apply the idea of limiting a region of significant gravitational influence, but this time considering in its definition the conditions of the encounter, in particular the relative velocity of the particle at the encounter. The same technique applied to the study of the temporary gravitational capture mechanism takes us to the definition of the regions of capture, whose limits are also given according to the relative velocity of the encounter and of the system's mass ratio. This study has resulted in a complete mapping of the influence and capture regions, considering systems with a mass ratio from 10^{-1} to 10^{-12}, based on the theory of the two-body problem and the circular restricted three-body problem, and culminating in the acquisition of the functions for the calculation of the influence radius and the capture radius, limits that are the borders of these regimes.

The structure of this paper is as follows. In Section 2, we present the initial considerations and the initial conditions of the problem. In Section 3, we present numerical results and discussions about the temporary gravitational capture. In Section 4, we present the results for the same technique applied to the study of the sphere of influence. In Section 5, we present our conclusions, with an overview of the results presented in the previous sections.

2 INITIAL CONSIDERATIONS

Three bodies are considered: M_1, the most massive body, here called the central body; M_2, a less massive body, having a circular orbit around M_1, here called the secondary body; M_3, a particle (P) of negligible mass, which also has an orbit around M_1. If M_1 is much larger than M_2, the largest part of the particle's movement around the central body is described according to the theory of the two-body problem. Thus, the restricted three-body problem is considered only when the particle approaches M_2. Therefore, the analysis of the energy of the two-body problem seems to be a good criterion to determine the regimes of gravitational capture or of significant influence of the secondary body.

For the integrations required for the calculation of this energy, two reference systems were introduced: the synodic and the inertial reference systems. The inertial reference system (ξ, η) is a fixed system, whose origin is in the barycentre of the system: $\mu_1 = 1 - \mu_2$ with $\mu_2 = M_2/(M_1 + M_2)$. The axis ξ is the axis along the line that connects M_1 to M_2 at the instant $t = 0$, which corresponds to the instant when M_1, M_2 and M_3 are aligned. The axis η is perpendicular to the orbital plane of the two masses. In this reference system, both M_1 and M_2 have a circular orbit around the barycentre of the system. Because of this characteristic, it is convenient to introduce the synodic reference system (X, Y) defined so as to follow the movement of the main masses. In this system, the direction of the axis X is chosen in such a way that the main bodies are always on it, and the axis Y is perpendicular to X. This system rotates with an angular velocity equal to the mean motion, n, of the primaries. From these definitions, we can conclude that when $t = 0$, the inertial and synodic systems coincide.

Fig. 1 illustrates the initial configuration considered. The distance d is the approach parameter, and corresponds to the distance between the particle and the secondary body when $t = 0$. Because in this instant the particle is on axis X, its initial position in the synodic system is given by

$$X = \mu_1 + d, \qquad Y = 0, \tag{1}$$

and its initial velocity components are

$$\dot{X} = 0, \qquad \dot{Y} = V_P - nX. \tag{2}$$

The particle–secondary body relative velocity (υ) is the difference between the particle's velocity (V_P) and the secondary body's velocity (V_2), which is

$$\upsilon = V_P - V_2. \tag{3}$$

Here, V_2 is the linear velocity of the secondary body, given by

$$V_2 = n\mu_1. \tag{4}$$

Thus, from equations (1)–(4) we have the initial conditions of the particle used in the integrations, given by

$$X = \mu_1 + d, \qquad Y = 0, \qquad \dot{X} = 0, \qquad \dot{Y} = \upsilon - d. \tag{5}$$

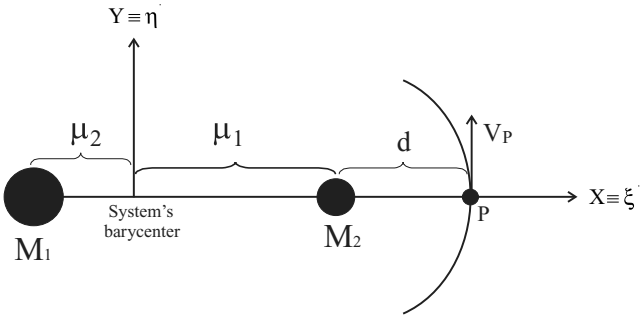

Figure 1. Initial configuration.

The numerical values that we input into the integrations are given in a system of adimensional unities, defined in such a way that the distance between the central body and the secondary body equals 1, as well as the sum of the masses of the system, which is $\mu = \mu_1 + \mu_2 = 1$. The system rotates with period 2π, and so the angular velocity of the rotation of the system is also unitary, or $n = 1$.

3 TEMPORARY GRAVITATIONAL CAPTURE

The gravitational capture mechanism has many applications in celestial mechanics. It was used, for instance, to justify the existence of the irregular satellites of the giant planets (Peale 1999). Later, it was shown that, in this problem, the increase in the mass of Jupiter was one of the factors responsible for making the capture permanent (i.e. satellites; Heppenheimer 1975; Heppenheimer & Porco 1977; Brunini 1995; Vieira Neto, Winter & Yokoyama 2004). It also has an important application in the techniques for manoeuvring with space vehicles, where orbital transfers are made by using gravitational interaction, resulting in the reduction of fuel consumption and, consequently, in the reduction of mission costs, which justifies the special interest in this phenomenon (Belbruno 1987, 1990, 1994; Belbruno & Miller 1993; Krish 1991; Krish, Belbruno & Hollister 1992; Miller & Belbruno 1991; Belbruno & Miller 1990; Yamakawa 1992; Yamakawa et al. 1993).

Gravitational capture can be understood as the phenomenon in which a particle approaches a massive body from a great distance and so remains for a lapse of time, not getting any further. This capture time depends on the problem being considered. Permanent capture is possible, for instance, in the restricted hyperbolic problem (Sizova 1952; Merman 1953). However, in the restricted circular and elliptical three-body problem, permanent capture is not possible (Fesenkov 1946; Yegorov 1960; Sung 1969; Tanikawa 1983), thus the name 'temporary gravitational capture'.

An important definition for the numerical approach to temporary gravitational capture presented in this paper is given by Yamakawa (1992). Yamakawa relates this phenomenon to the two-body problem energy, and says that if the energy of a particle relative to a celestial body is initially positive (hyperbolic movement) and then it becomes negative (elliptical movement) it can be considered that capture has occurred. Thus, while the particle is temporarily captured by the secondary body, the relative energy between these two bodies will be negative. When it escapes from that capture and starts to orbit the central body, the particle–secondary body energy will be positive. This condition is shown in the example of Fig. 2, where we can see that the particle–secondary body energy of a particle with $\upsilon = 0.0050$ in a system with mass ratio $\mu_2 = 10^{-7}$, which passes at a distance $d = 0.00287$, is initially negative, but after a lapse of time it becomes positive (Fig. 2a). According to the definition of Yamakawa, this means that it was temporarily captured and then escaped, going to an orbit relative to the central body. This situation is better visualized in a graph of the trajectory of the particle in a planetocentric system, which is a fixed system with the secondary body in the origin. We can initially see the particle performing laps around the secondary body, which means it is captured, but later it backs off, indicating that it has escaped (Fig. 2b). Fig. 2(c) shows an interesting behaviour of the two-body energy (particle–central body), which agrees with what was said above. We can see that while the particle remained captured, this energy varied greatly, because of its approaching and backing off to the secondary body movement in that period of time. Some time after the moment at which the particle escaped, indicated by a point, the energy becomes practically constant, indicating that the secondary body stopped influencing the particle and the problem became essentially a two-body problem (particle–central body).

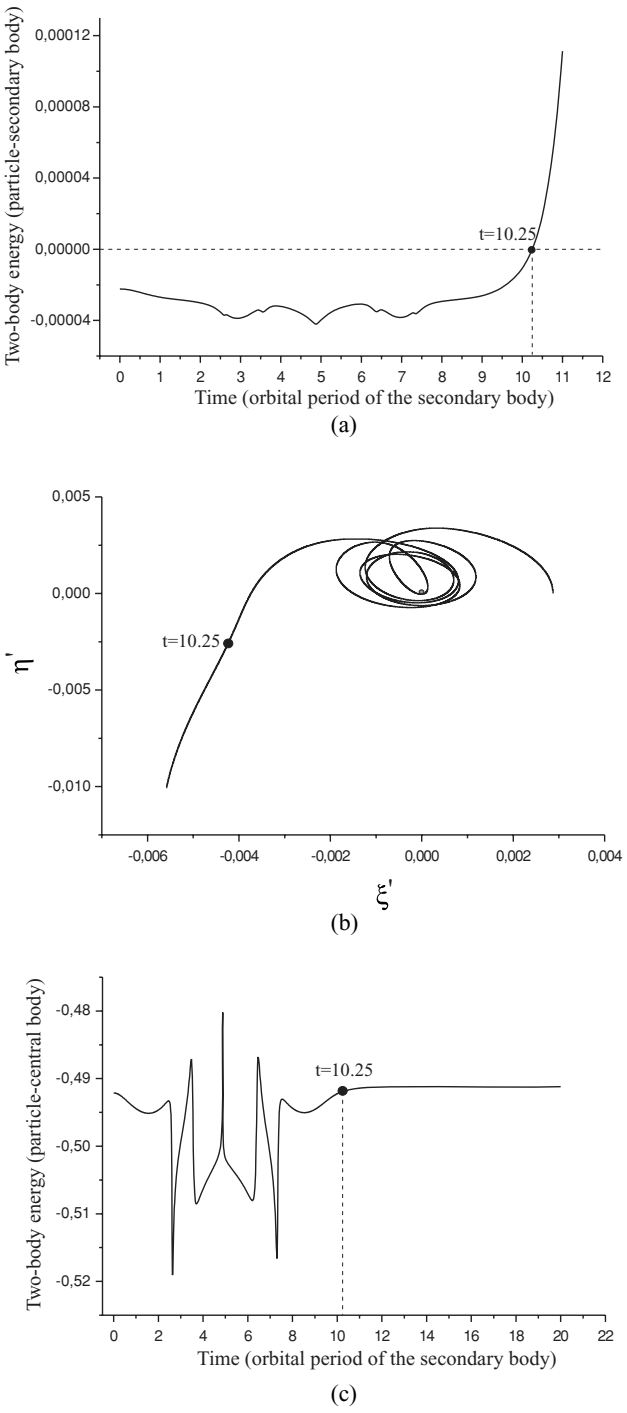

Figure 2. Particle with $\upsilon = 0.0050$, $d = 0.00287$ and $\mu_2 = 10^{-7}$. (a) Two-body problem (particle–secondary body) energy, for integration time equal to 11 orbital periods of the secondary body. (b) Trajectory in a planetocentric system, for integration time equal to 11 orbital periods of the secondary body. (c) Two-body problem (particle–central body) energy, for integration time equal to 20 orbital periods of the secondary body.

Thus, in this section we monitor these energies, considering systems with a mass ratio from 10^{-1} to 10^{-12}, and particles with different initial relative velocities. We have found the value of the

approach parameter d when the transition between capture and no-capture occurs, defined as the capture radius ($R_{\rm Cap}$).

3.1 Numerical integrations

Using the Gauss–Radau integrator (Everhart 1985), a routine was written to perform numerical integrations that provide the value of the two-body energy (particle–secondary body) in a dynamics of three bodies, along the integration period. In this program, we input the equations that define the initial conditions given by equation (5), with the system's mass ratio, with the value of the initial velocity of the particle relative to the secondary body (υ) and with the approach parameter d.

The method applied consists of keeping the system's mass ratio fixed, putting a particle with the initial relative velocity to the secondary body υ also fixed in this system, and then increasing the value of the distance d from the secondary body that it passes. For each value of d, we analysed, through the variation of the two-body problem energy and the trajectory of the particle in the planetocentric system, whether the capture occurred. The value of d, for which there is no capture, is then considered as the capture radius ($R_{\rm Cap}$) for particles with the initial relative velocity and the mass ratio fixed previously.

The following example illustrates the application of this method. The same particle as in the example presented in Fig. 2 was considered, with $\upsilon = 0.0050$, $\mu_2 = 10^{-7}$ and for an integration time equal to five orbital periods of the secondary body. The problem starts with the value $d = 0.00287$, which, as shown before, results in a particle initially captured, as shown in Figs 3(a) and (b). So, increasingly, the value used for d, up to the value for which the particle is no longer captured, is found, as shown Figs 3(c) and (d) (i.e. $d = 0.00289$). From this example, we can conclude that a particle with an initial relative velocity equal to $\upsilon = 0.0050$, in a system whose mass ratio is 10^{-7}, will be captured if it passes at a distance less than 0.00289 from the secondary body, and it will not be captured if the distance is larger than this value. Thus, the value of d that limits this condition (i.e. $d = 0.00289$) is then considered to be the capture radius ($R_{\rm Cap}$).

This procedure, applied to a large number of initial conditions, allows the acquisition of a model in which the capture radius is obtained as a function of υ and μ_2 [i.e. $R_{\rm Cap}(\upsilon, \mu_2)$].

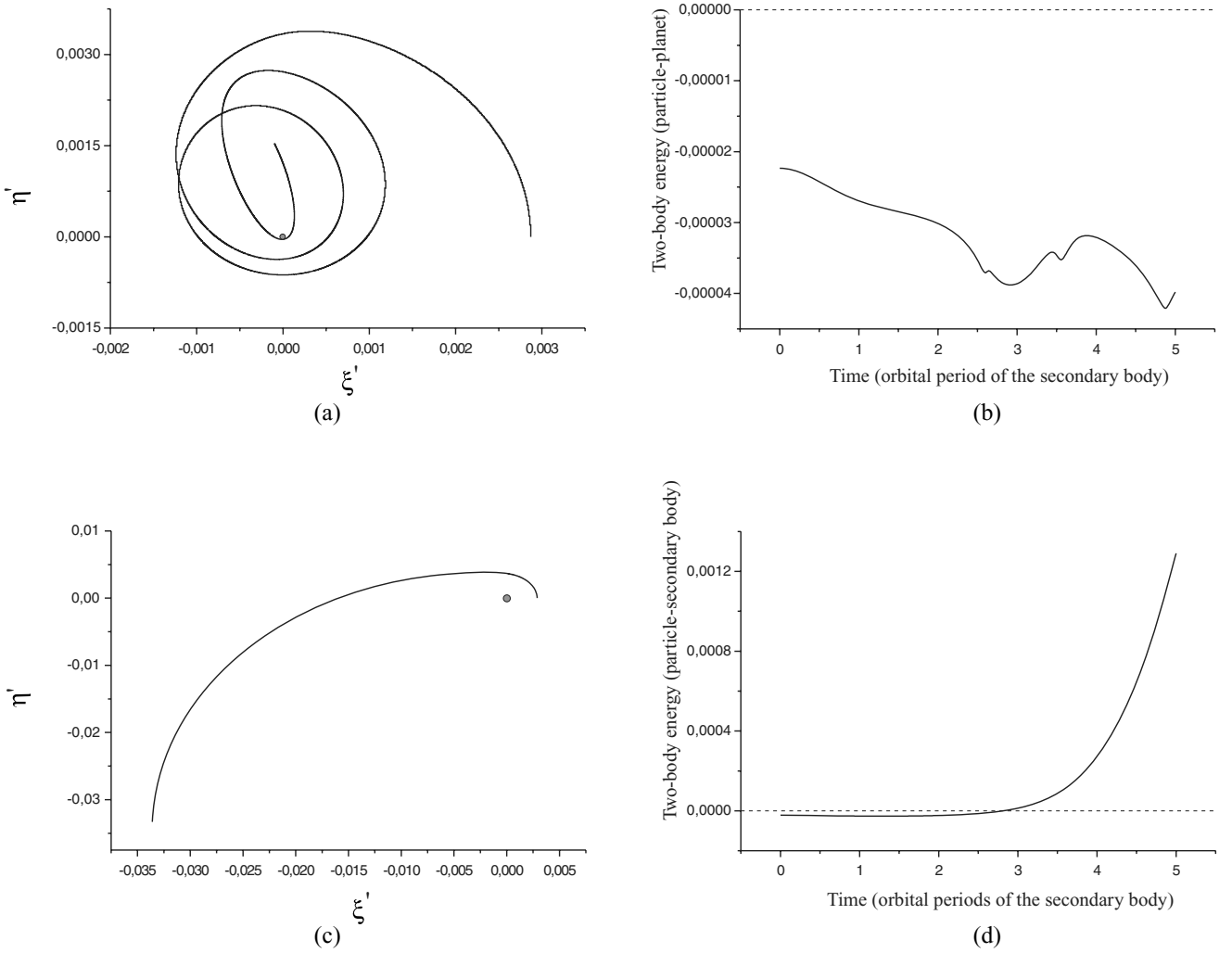

Figure 3. Particle with $\upsilon = 0.0050$ in a system with a mass ratio of 10^{-7}. (a) Trajectory of the particle in the planetocentric system for $d = 0.00287$. (b) Variation of the two-body problem energy (particle–secondary body) for $d = 0.00287$. (c) Trajectory of the particle in the planetocentric system for $d = 0.00289$. (d) Variation of the two-body problem energy (particle–secondary body) for $d = 0.00289$.

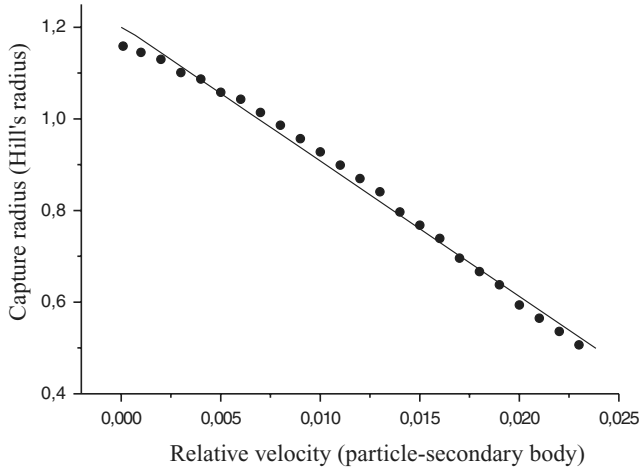

Figure 4. Capture radius as a function of the particle–secondary body relative velocity, to $\mu_2 = 10^{-6}$.

We limited our study to positive initial relative velocities and $d \leq 0.5$ Hill radius, as such limits are enough to guarantee its application.

3.2 Numerical modelling of temporary gravitational capture

Integrations for 12 mass ratios, from 10^{-1} to 10^{-12}, were made. These values basically comprise the mass ratios found in the Solar system, as well as in the Pluto–Charon system, where the mass ratio is about 10^{-1}, passing to the Sun–planets mass ratio, and ending up with extremely small mass ratios, of about 10^{-12}, such as those that can be found in the system formed between Saturn and its smaller satellites.

For each of these mass ratios, after a significant number of simulations, a curve like that shown in Fig. 4, made for $\mu_2 = 10^{-6}$, was obtained. Each point of this graph was obtained following the steps presented in Section 3.1.

A linear fit (solid line) takes us to the equation of this curve, which corresponds to the function for the calculation of the capture radius as a function of the relative velocity, $R_{\rm Cap}(\upsilon)$, given in the Hill radius. For the system with mass ratio 10^{-6}, this is given by

$$R_{\rm Cap}(\upsilon) = 1.208 - 29.847\upsilon. \quad (6)$$

The curves for all the mass ratios are shown in Fig. 5. As in the example of Fig. 4 and equation (6), each of these curves provides a function

$$R_{\rm Cap}(\upsilon) = A_{\rm Cap} - B_{\rm Cap}\upsilon, \quad (7)$$

with their respective coefficients $A_{\rm Cap}$ and $B_{\rm Cap}$ given in columns 2 and 3 of Table 1. With these results, we already have the capture radius as a function of the relative velocity. Now, we want to obtain a single function that expresses it, not just depending on this velocity, but also on the system's mass ratio.

Primarily, we note that the coefficient $A_{\rm Cap}$ varies very little as a function of the mass ratio, being almost constant, around the mean value:

$$A_{\rm Cap} = 1.219 \pm 0.036. \quad (8)$$

Unlike $A_{\rm Cap}$, it is noticeable that the coefficient $B_{\rm Cap}$ varies considerably, as the mass ratio decreases. Thus, it is necessary to express this as a function of the mass ratio. In order to do this, we consider

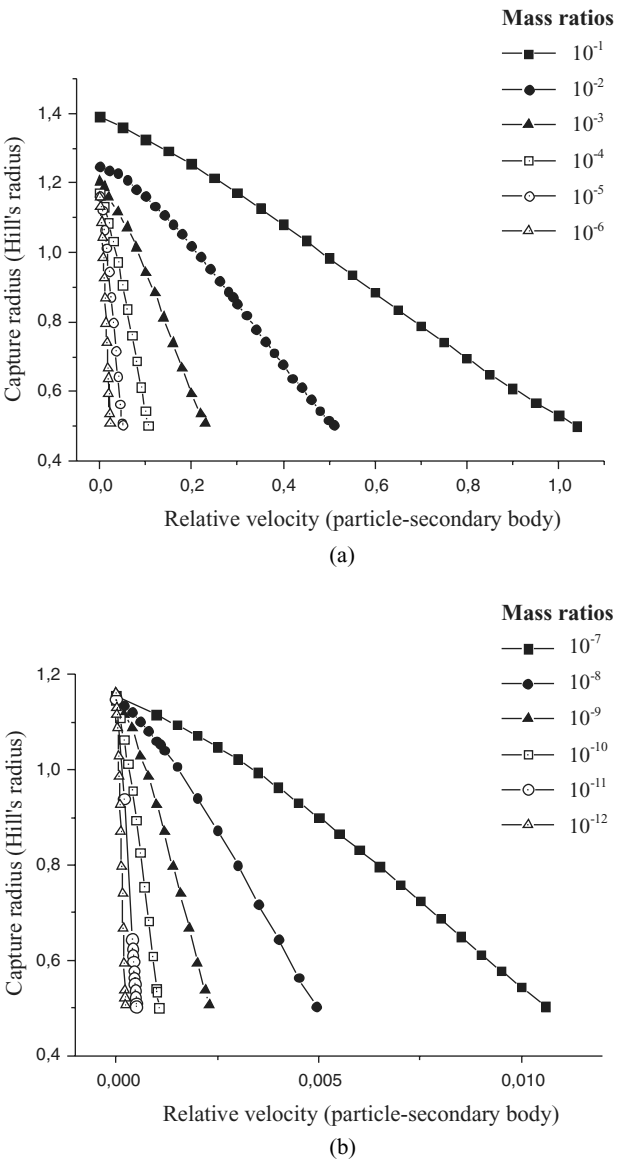

Figure 5. Capture radius as a function of the relative velocity: (a) mass ratios from 10^{-1} to 10^{-6}; (b) mass ratios from 10^{-7} to 10^{-12}.

Fig. 6, created using the data from columns 1 and 3 of Table 1. A logarithmic scale on the two axes was adopted, resulting in a straight line. Such behaviour suggests a relation of the kind

$$B_{\rm Cap}(\mu_2) = \alpha\mu_2^{\beta}. \quad (9)$$

The coefficients α and β are obtained through a linear fit in this curve: $\alpha = 0.3532 \pm 0.0162$ and $\beta = -0.3246 \pm 0.0027$. Thus, the coefficient $B_{\rm Cap}$ relates to the mass ratio μ_2 through

$$B_{\rm Cap}(\mu_2) \approx 0.35\mu_2^{-0.32}. \quad (10)$$

The errors between the empirical values of $B_{\rm Cap}$ and the values obtained through this equation are given in Table 1. Therefore, from equations (8) and (10), we found that the mathematical function that expresses the capture radius as a function of the mass ratio and the relative velocity is approximately given by

$$R_{\rm Cap}(\upsilon, \mu_2) \approx 1.2 - 0.35\mu_2^{-0.32}\upsilon. \quad (11)$$

The unity of the capture radius calculated through this function is the Hill radius.

Table 1. Coefficients A_{Cap} and B_{Cap} of equation (7) and the values for the coefficient B_{Cap} obtained through a linear fit with their respective errors.

Mass ratio	Coefficient A_{Cap}	Coefficient B_{Cap}	Coefficient B_{Cap} linear fit	Error per cent
10^{-1}	1.301	0.897	0.746	20.2
10^{-2}	1.282	1.573	1.575	−0.2
10^{-3}	1.232	3.099	3.325	−6.8
10^{-4}	1.216	6.572	7.021	−6.4
10^{-5}	1.209	14.042	14.826	−5.3
10^{-6}	1.208	29.847	31.306	−4.7
10^{-7}	1.199	63.688	66.103	−3.7
10^{-8}	1.195	136.532	139.579	−2.2
10^{-9}	1.201	295.063	294.728	0.1
10^{-10}	1.190	630.978	622.330	1.4
10^{-11}	1.195	1363.655	1314.077	3.8
10^{-12}	1.201	2942.123	2774.730	6.0

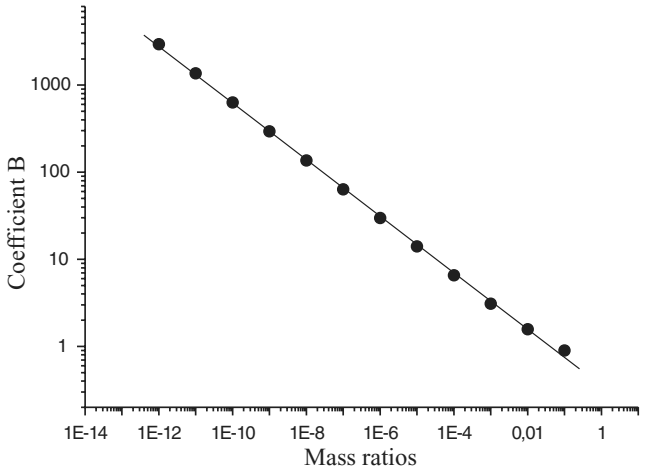

Figure 6. Coefficient B_{Cap} as a function of the mass ratio, in a logarithmic scale.

3.3 Analytical approach

In order to interpret our numerical results, in this section we make a comparison between these and what is expected from the circular restricted three-body problem. From such a theory, it is known that

$$V^2 = 2U - C, \tag{12}$$

where V^2 is the square of the particle's velocity in the synodic reference system, C is the Jacobi constant and U is called the 'pseudo-potential', given by

$$U = \frac{1}{2}(X^2 + Y^2) + \frac{\mu_1}{r_1} + \frac{\mu_2}{r_2}. \tag{13}$$

Considering the particle's initial condition, and that d and μ_2 are very small, the approximations $\mu_1 \approx 1$ and $r_1 \approx 1$ are valid. Using this consideration in equation (13) we have that

$$2U \approx 3 + \frac{2\mu_2}{r_2}. \tag{14}$$

For the particle, $r_2 \approx d$, and so, from equations (12) and (14):

$$V^2 \approx 3 + \frac{2\mu_2}{d} - C. \tag{15}$$

However, if a capture is required, the value of the Jacobi constant C should be approximately the value of such a constant at the second Lagrangian point $C(L_2)$. Considering again the approximations

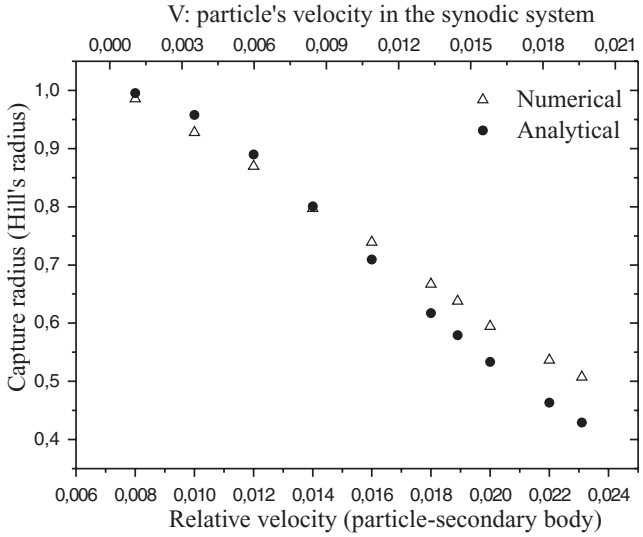

Figure 7. Comparison between the numerical and analytical models for capture radius, as a function of the velocity (V or υ), considering $\mu_2 = 10^{-6}$.

above, it is possible to show that for this Lagrangian point, $r_2 \approx (\mu_2/3)^{1/3}$, which is the definition of the Hill sphere of influence radius (R_H), (see, for example, Valtonen & Karttunen 2006). So, from equations (12) and (14), and remembering that for L_2 in the synodic reference system, $V^2 = 0$, we have

$$C(L_2) \approx 3 + \frac{2\mu_2}{R_H}. \tag{16}$$

Combining equation (16) with equation (15), it is possible to obtain a function that approximately gives d for capture cases in the Hill radius, as a function of the particle's velocity in the synodic system, according to the three-body restricted problem theory. This will be

$$\frac{d}{R_H} \leq \frac{1}{1 + \left(V^2 R_H / 2\mu_2\right)}. \tag{17}$$

This value corresponds to the distance for which, given a velocity V, $C(L_2)$ remains constant. So, when $V = 0$, $d = 1R_H$, which is exactly r_2 for the Lagrangian point L_2. The symbol ($\leq$) in this equation indicates that the numerical value obtained represents the limit of a region where the capture occurs.

Now we compare this analytical model with the numerical model given in Section 3.2. With this aim, in equation (17) we used the values for the relative velocity presented in Fig. 5, remembering that $V^2 = \dot{X}^2 + \dot{Y}^2 = (\upsilon - d)^2$, according to equation (5). Fig. 7 shows the numerical and analytical results for $\mu_2 = 10^{-6}$ considering only prograde cases. We have found that these two models agree with each other for small velocities, but as this value increases, the difference becomes larger. For the mass ratios considered in Fig. 7, for instance, the largest difference is about 15 per cent, which corresponds to the largest velocity. This same characteristic is observed for the other mass ratios. In all cases studied, the difference is about 20 per cent. The largest difference occurs for $\mu_2 = 10^{-2}$, with a difference of 21.3 per cent.

4 SPHERE OF INFLUENCE

In the previous section, we have shown that, for particles with a given initial relative velocity, there is a distance limit that determines whether they will be captured or not; this is called the capture

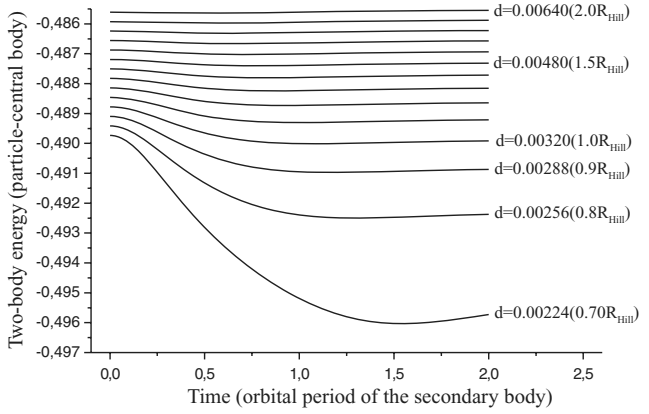

Figure 8. Variation of the two-body problem energy (particle–central body) as a function of the time, to a particle with $\upsilon = 0.0080$ and $\mu_2 = 10^{-7}$.

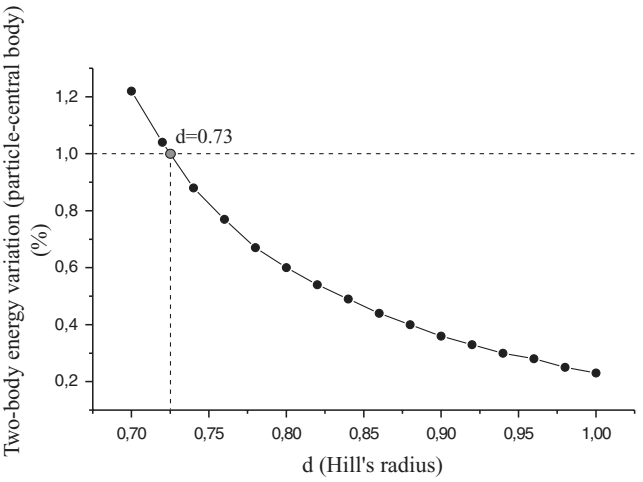

Figure 9. Variation of energy (particle–central body) as a function of the approach parameter d, to a particle with $\upsilon = 0.0080$ and to $\mu_2 = 10^{-7}$.

radius ($R_{\rm Cap}$). So, if the approach parameter is smaller than $R_{\rm Cap}$, the particle is captured. For values of d larger than $R_{\rm Cap}$, there will be, initially, a region where the particle is no longer captured, but d is small enough for the secondary body to exercise a significant influence over it. Nevertheless, as d increases, the effect of the secondary body perturbation decreases, as the initial particle–secondary body relative velocity remains the same. So we have a two-body problem (particle–central body) with almost constant energy. This evolution is shown in Fig. 8, for a particle with initial relative velocity $\upsilon = 0.0080$ in a system with mass ratio 10^{-7}. In this example, the integration starts with the first value of the approach parameter, which does not result in the capture of the particle for this velocity. Then, the value d is increased. For each of these values, the system is integrated in time ($t = 2$ orbital periods of the secondary body). We can see that for the smallest d values, the variation of energy is very large. As d increases (i.e. as the particle gets further from the secondary body), the smaller the variation of energy provided by the encounter is, and so on, until it becomes practically constant, indicating that the particle has left the sphere of influence of the secondary body.

Next, we compute the variation of energy ΔE provided by each of these encounters. To calculate such a variation, we consider the two-body energy (particle–secondary body), when $t = 0$, here called $E_{\rm initial}$, and the same energy value at the final integration time, called $E_{\rm final}$, in such way that

$$\Delta E = \frac{(E_{\rm initial} - E_{\rm final})}{E_{\rm initial}} 100 \,\text{per cent}. \qquad (18)$$

This variation is the parameter that will tell us whether the particle with the initial conditions given was significantly influenced by the encounter with the secondary body. The question is, what ΔE value should be considered as a limit for the secondary body influence? This is an arbitrary value, and it will depend on the characteristics of the problem being studied. In this work, we fixed $\Delta E =$ 1.0 per cent for a significant influence of the secondary body. Thus, in our method, if the integration for a given value of d results in an energy variation larger than 1.0 per cent, we consider that the particle is within the sphere of influence of the secondary body. If this variation is smaller than 1.0 per cent, we consider that it is outside that sphere of influence. The exact value of d for which this energy variation occurs becomes the influence radius, $R_{\rm Inf}$. This value of d is obtained through a graph like that in Fig. 9, which shows how the energy of the two-body problem (particle–central body) varies as a function of the approach parameter, made from the encounters exemplified in Fig. 8, taking intermediary values for d, in the interval from 0.7 to 1.0 Hill radius. The dotted line indicates when the variation of energy is 1.0 per cent.

Thus, the method for this study consists of keeping the system's mass ratio and the initial relative velocity fixed, and for these conditions varying the approach parameter. For each of these values, the system is integrated, and the variation of energy is computed. These data are organized in a graph like that in Fig. 9, and from this we can obtain the exact d value that leads to an energy variation with percentage equal to 1.0 per cent, which is then considered the radius of influence, $R_{\rm inf}$

4.1 Numerical integrations

In the numerical integrations of this study, the routine used in the case of the temporary gravitational capture was adapted, so that this time it can provide the value of the energy of the two-body problem (particle–central body), in a dynamics of three bodies, along the period of integration. In this program, we input the same equations that define the initial conditions given by equation (5), with the system's mass ratio, the initial relative velocity (υ), the value of the approach parameter d and the integration time equal to two orbital periods of the secondary body. As before, we limited our study to prograde movements, and to $d \leq 0.5$ Hill radius.

4.2 Results

4.2.1 Systems with mass ratio from 10^{-1} *to* 10^{-6}

The integrations made for these mass ratios have shown that there is no region where we can consider that the gravitational influence of one of the primary bodies can be neglected. In fact, the secondary body will always influence the particle's movement. This conclusion comes straight from the analysis of the energy of the two-body problem (particle–central body), as shown in Fig. 10(a), made for a particle with $\upsilon = 0.370$, $d = 0.104$ (0.70 Hill radius) and for $\mu_2 = 10^{-2}$. We can see that the two-body problem energy does not remain constant, as predicted by the theory, but continues to vary along the integration period, even when the particle is distant from the secondary body, as Fig. 10(b) shows. This means that, for these mass ratios, the approach of the two-body problem, with $\Delta E <$ 1 per cent, cannot be made. So the problem must be always treated

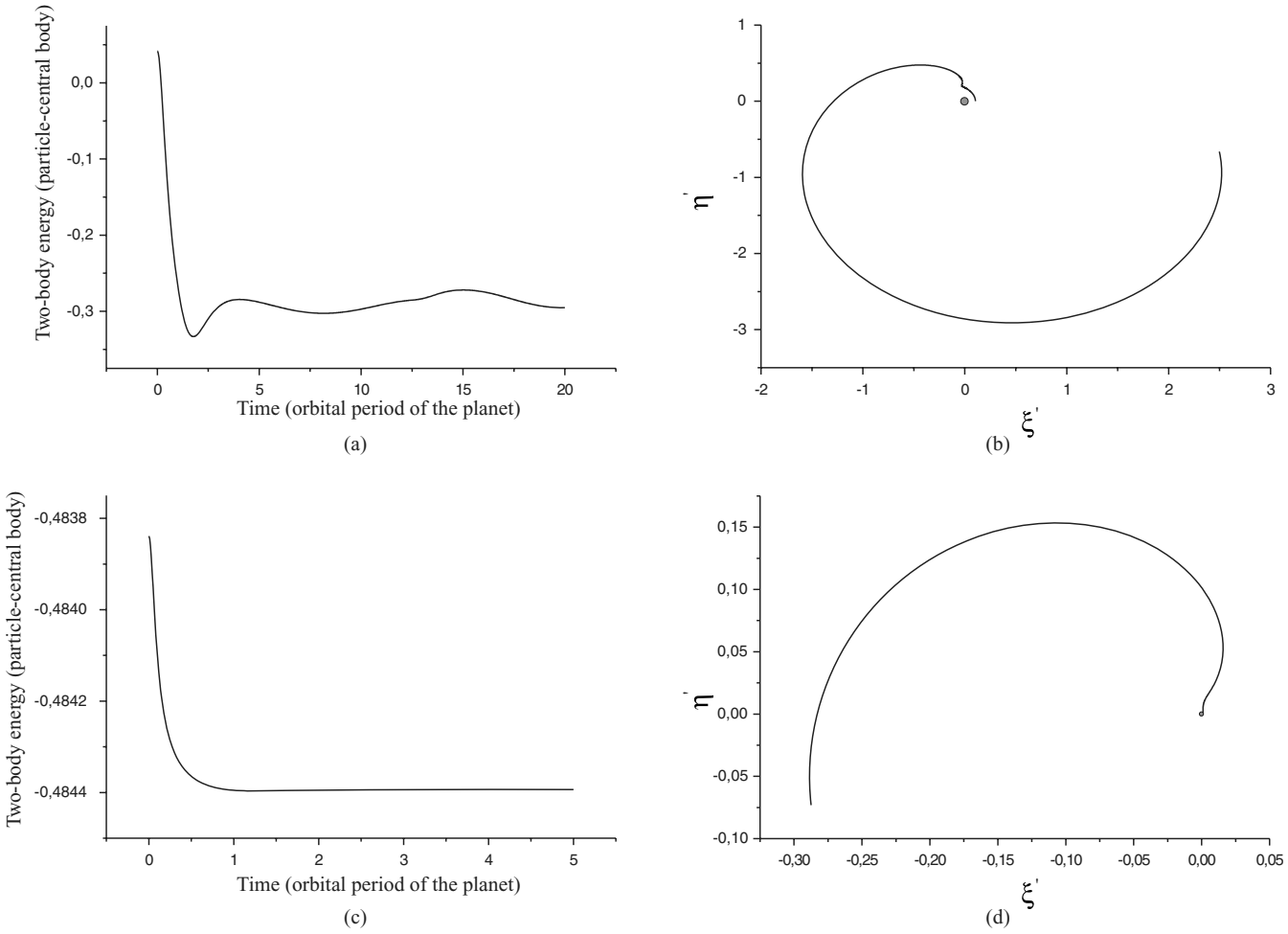

Figure 10. (a) Variation of the two-body problem energy (particle–central body). (b) Trajectory of the particle in the planetocentric system, for a particle initially with $\upsilon = 0.370$, $d = 0.104$ (0.70 Hill radius) in a system with mass ratio 10^{-2}. (c) Variation of the two-body problem energy (particle–central body). (d) Trajectory of the particle in the planetocentric system, for a particle initially with $\upsilon = 0.015$, $d = 0.00105$ (0.70 Hill radius) in a system with mass ratio 10^{-8}.

as a three-body problem, therefore not applying to it the concept of the sphere of influence for these cases.

4.2.2 *Systems with mass ratio from* 10^{-6} *to* 10^{-12}

For these mass ratio values, the approach of the two-body problem with $\Delta E < 1$ per cent becomes valid. Fig. 10(c), which was made considering a particle with $\upsilon = 0.015$, $d = 0.00105$ (0.70 Hill radius) in a system with mass ratio 10^{-8}, confirms this behaviour. We can see that, initially, the energy varies, indicating the action of the secondary body, but later it becomes practically constant, showing that the secondary body stopped significantly influencing its movement. Then, we essentially have a two-body problem (particle–central body), with constant energy, as can be seen in Fig. 10(d).

From our simulations we found that for $2 \times 10^{-8} \leq \mu_2 \leq 2 \times 10^{-6}$ the numerical modelling for the sphere of influence that we propose works well. Fig. 11 shows the results for these mass ratios. Each point of this graph was obtained through the method described in Sections 4.1 and 4.2. Through a linear fit to each of these curves, we can obtain the equations of these curves, which correspond to the functions for the calculation of the radius of influence as a function of the relative velocity (υ). Because of its linear characteristics, it will have the form

$$R_{\rm Inf}(\upsilon) = A_{\rm Inf} - B_{\rm Inf}\upsilon, \tag{19}$$

with the respective coefficients $A_{\rm Inf}$ and $B_{\rm Inf}$ given in columns 2 and 3 of Table 2. The coefficient $A_{\rm Inf}$ is approximately constant, around the mean value,

$$A_{\rm Inf} = 1.005 \pm 0.035, \tag{20}$$

while the coefficient $B_{\rm Inf}$ varies significantly with the mass ratio. With a graph such as that in Fig. 6, we find that this variation also follows a relation of the kind

$$B_{\rm Inf}(\mu_2) = \alpha \mu_2^{\beta}, \tag{21}$$

when we consider a linear fit in such a curve. In this case, the coefficients α and β are $\alpha = 0.00057 \pm 0.00023$ and $\beta = -0.68346 \pm 0.02622$, and so

$$B_{\rm Inf}(\mu_2) \approx 0.00057\mu_2^{-0.68}. \tag{22}$$

However, it will be

$$B_{\rm Inf}(\mu_2) = 10^{\alpha}\mu_2^{[\beta+\delta\log(\mu_2)]} \tag{23}$$

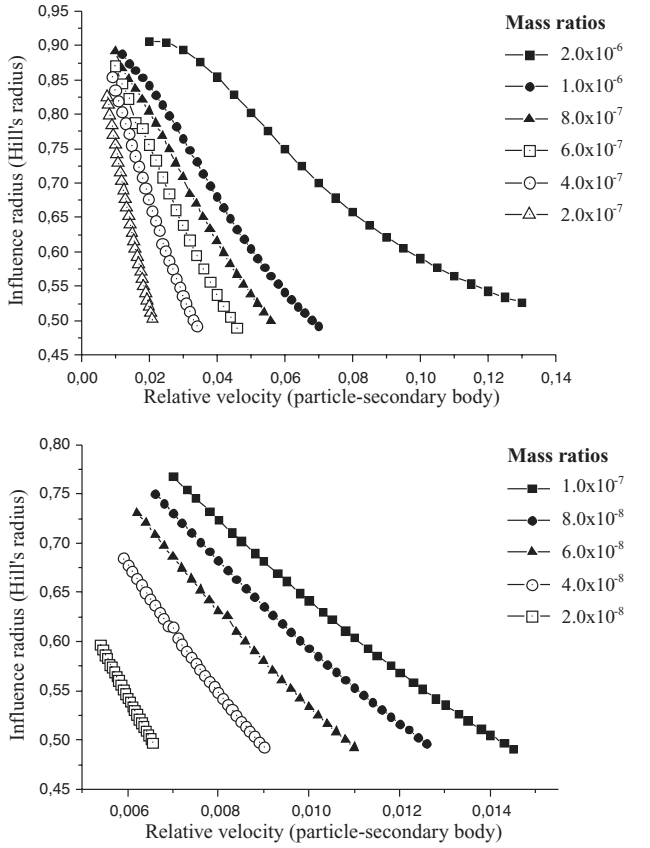

Figure 11. Influence radius as a function of the relative velocity υ: (a) mass ratios from 2.0×10^{-6} to 2.0×10^{-7}; (b) mass ratios from 1.0×10^{-7} to 2.0×10^{-8}.

when a quadratic fit is considered, with $\alpha = -9.6050 \pm 0.5607$, $\beta = -2.6002 \pm 0.1686$ and $\delta = -0.1432 \pm 0.01259$, in such way that

$$B_{\rm Inf}(\mu_2) \approx (2.48 \times 10^{-10})\mu_2^{-2.60-0.14\log(\mu_2)}. \quad (24)$$

The quadratic fit leads to smaller errors when compared to the linear fit, leading, in this way, to higher precision in the results, as the values in Table 2 show. With these considerations, we finally have that the radius of the sphere of influence as a function of the relative velocity and the mass ratio of the system is

$$R_{\rm Inf}(\upsilon, \mu_2) = 1.00 - 0.00057\mu_2^{-0.68}\upsilon, \quad (25)$$

or, more precisely,

$$R_{\rm Inf}(\upsilon, \mu_2) = 1.00 - (2.48 \times 10^{-10})\mu_2^{-2.60-0.14\log(\mu_2)}\upsilon \quad (26)$$

when the quadratic fit is considered.

We note that equations (25) and (26) are valid for $2.0 \times 10^{-8} \leq \mu_2 \leq 2.0 \times 10^{-6}$.

For the values of $\mu_2 < 2.0 \times 10^{-8}$, we found that $\Delta E < 1$ per cent will occur only if $d < 0.5$ Hill radius. This is because as the mass ratio decreases, the particle must approach the secondary body, in order for a variation of 1.0 per cent in energy to occur, as the initial relative velocity remains fixed. We can imagine that, being so small, these bodies with such mass ratios will influence very little the movement of the particle. The central body will prevail practically along the whole orbital period of the particle. So, we have essentially a problem of two bodies (particle–central body), weakly modified by the secondary body, only when the particle passes extremely near it. This means that the sphere of influence, in this case, considering our approach, does not exist in practice.

5 CONCLUSION

In this paper, we have introduced an approach to identify the sphere of influence and the capture radius as a function of the encounter velocity and the mass ratio of the primaries.

The capture regions are well determined with the limits of this regime given by equation (11), which provides what we have defined as the capture radius, $R_{\rm Cap}$.

The influence radius is defined according to a measure of the variation of the two-body energy (particle–secondary body). Considering $\Delta E = 1.0$ per cent as the border of the influence region, we have found that there are basically three different regimes.

For large mass ratios, $10^{-6} \leq \mu_2 \leq 10^{-1}$, we have concluded that the secondary body will constantly influence the movement of the particle. Therefore, the two-body problem (particle–central body) approach is not valid and, consequently, the idea of the sphere of influence no longer makes sense. So, a particle moving in these systems will have its capture possible, or will have its movement essentially described by the three-body problem, depending on the distance of the encounter.

For intermediary mass ratios, $2.0 \times 10^{-8} \leq \mu_2 \leq 2.0 \times 10^{-6}$, we have a region where the secondary body temporarily dominates the

Table 2. Coefficients $A_{\rm Inf}$ and $B_{\rm Inf}$ of equation (19) and the values obtained through a linear and quadratic fit for $B_{\rm Inf}$ with their respective errors.

Mass ratio	Coefficient $A_{\rm Inf}$	Coefficient $B_{\rm Inf}$	Coefficient $B_{\rm Inf}$ linear fit	Error (per cent)	Coefficient $B_{\rm Inf}$ quadratic fit	Error (per cent)
2.0×10^{-8}	1.06	85.93	103.659	17.1	84.082	2.2
4.0×10^{-8}	1.05	62.16	64.545	−3.7	62.063	0.2
6.0×10^{-8}	1.04	50.10	48.923	2.4	50.543	−0.9
8.0×10^{-8}	1.02	42.50	40.190	5.7	43.153	−1.5
1.0×10^{-7}	1.02	36.92	34.505	7.0	37.903	−2.6
2.0×10^{-7}	1.00	24.19	21.485	12.6	24.352	0.7
4.0×10^{-7}	0.98	14.68	13.378	9.7	14.738	0.4
6.0×10^{-7}	0.96	10.74	10.140	5.9	10.686	0.5
8.0×10^{-7}	0.97	8.75	8.330	5.0	8.402	4.1
1.0×10^{-6}	0.98	7.24	7.152	1.2	6.923	4.6
2.0×10^{-6}	0.97	3.46	4.453	−22.3	3.647	5.1

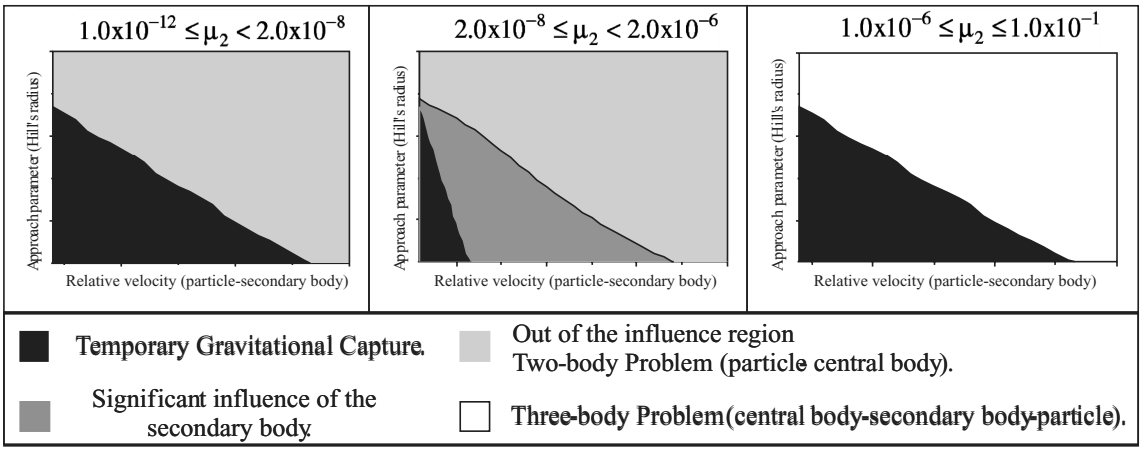

Figure 12. Diagrams showing the capture and influence regions as a function of the mass ratios, relative velocity and the distance of the encounter. Their limits are determined by equation (11) for capture and equations (25) or (26) for the influence radius.

dynamics of the particle. For these values, a model for the sphere of influence was obtained. The radius computed as a function of the relative velocity and the mass ratio is given by equation (25), or, more precisely, by equation (26).

For mass ratios $2.0 \times 10^{-12} \leq \mu_2 \leq 1.0 \times 10^{-8}$, we have shown that the secondary body will significantly influence the particle only if it goes too close to the secondary body. For these cases, the sphere radius will always be smaller than 0.5 Hill radius. Thus, a particle with a given velocity in these systems will either be captured or will essentially be in a Keplerian orbit around the central body, which will be weakly disturbed only when it goes very close to the secondary body.

Fig. 12 provides an overview of this mapping of the capture and influence regions in the interval of mass ratios considered, as a function of the distance d and the relative velocity of the encounter. In these diagrams, the borders of influence or capture are determined by equation (11) for capture and equations (25) or (26) for the influence radius. These always start with values higher than 0.5 Hill radius, which was imposed by the method, and the interval of velocities will depend on each case being studied, as Figs 5 and 11 show.

ACKNOWLEDGMENTS

This work was funded by Capes, CNPq and Fapesp. This support is gratefully acknowledged. The authors are also grateful to an anonymous referee for suggestions that significantly improved the paper.

REFERENCES

Belbruno E. A., 1987, in Kuang Y. Z., Shen G. Q., Yang S. T., eds, Proc. 19th International Electric Propulsion Conference. Institute of Aeronautics and Astronautics, Washington, DC

Belbruno E. A., 1990, in Thompson R. C., ed. AIAA/AAS Astrodynamics Conference. Institute of Aeronautics and Astronautics, Washington, DC, p. 179

Belbruno E. A., 1994, J. Br. Interplanet. Soc., 47, 73

Belbruno E. A., Miller J. K., 1990, JPL IOM-904-1752, A Ballistic Lunar Capture Trajectory for the Lunar Observer Mission. Jet Propulsion Laboratory, Pasadena, CA

Belbruno E. A., Miller J. K., 1993, J. Guidance Control Dyn., 16, 770

Broucke R. A. 1988, in Wercinski P. F., ed., AIAA/AAS Astrodynamics Conference. American Institute of Aeronautics and Astronautics, Washington, DC, p. 69

Brunini A., 1995, Earth Moon Planets, 71, 281

Domingos R. C., Winter O. C., Yokoyama T., 2006, MNRAS, 373, 1227

Dunne J. A., 1974, Sci, 185, 141

Everhart E., 1985, in Carusi A., Valsecchi G. B., eds, Dynamics of Comets: Their Origin and Evolution. Reidel, Dordrecht, p. 185

Fesenkov V. G., 1946, AZh, 23, 45

Hamilton D. P., Burns J. A., 1991, Icarus, 92, 118

Heppenheimer T. A., 1975, Icarus, 24, 172

Heppenheimer T. A., Porco C., 1977, Icarus, 30, 385

Hill G. W., 1878, Am. J. Math., 1, 5

Kohlhase C. E., Penzo P. A., 1977, Space Sci. Rev., 21, 77

Kornet K., Wolf F., Rózyczka M., 2006, A&A, 458, 661

Krish V., 1991, Dissertation, Massachusetts Institute of Technology, Cambridge, MA, USA

Krish V., Belbruno E. A., Hollister W. M., 1992, in Upadhyay T. N., Cotterill S., Deaton A. W., eds, AIAA/AAS Astrodynamics Conference. American Institute of Aeronautics and Astronautics, Washington, DC, p. 439

Merman G. A., 1953, Bull. Inst. Teor. Astron., 5, 325

Miller J. K., Belbruno E. A., 1991, in AAS/AIAA Space Flight Mechanics Meeting 1. American Institute of Aeronautics and Astronautics, Washington, DC, p. 97

Peale S. J., 1999, ARA&A, 37, 533

Peralta F., Flanagan S., 1995, Control Eng. Pract.e, 3, 1603

Prado A. F. B. A., 2001, Trajetórias Espaciais e Manobras Assistidas por Gravidade. INPE, São José dos Campos

Roy A. E., 1988, Orbital Motion, 3rd edn. Adam Hilger, Bristol

Sizova O. A., 1952, Dokl. Akad. Nauk SSSR, 86, 485

Sung C.-H., 1969, PhD thesis, Yale Univ.

Tanikawa K., 1983, Celest. Mech., 29, 367

Vieira Neto E., Winter O. C., Yokoyama T., 2004, A&A, 414, 727

Wenzel K. P., Marsden R. G., Page D. E., Smith E. J., 1992, A&AS, 92, 207

Yamakawa H., 1992, PhD thesis, Univ. Tokyo

Yamakawa H., Kawaguchi J., Ishii N., Matsuo H., 1993, in AAS/AIAA Astrodynamics Specialist Conference. American Institute of Aeronautics and Astronautics, Washington, DC

Yegorov V. A., 1960, The Capture Problem in the Three-Body Restricted Orbital Problem. (NASA Technical Translation F-9). NASA, Washington, DC, p. 16

Valtonen M., Karttunen H., 2006, The Three-Body Problem. Cambridge Univ. Press, New York, p. 131

This paper has been typeset from a TEX/LATEX file prepared by the author.